Electronic Supplementary Information

From boron cluster to gold cluster: A New Label-free Colorimetric Sensors

Bin Qi, Chenchen Wu, Ling Xu, Wenjing Wang, Jin Cao, Jun Liu, Shuai Zhang, Detlef Gabel, Haibo Zhang* and Xiaohai Zhou*

College of Chemistry and Molecular Sciences, Wuhan University, Wuhan, 430072, China.

Table of Contents

1. General materials and methods

Materials and reagents: Hydrogen tetrachloride gold(Ⅲ) tetrahydrate ($HAuCl_4 \cdot 4H_2O$, 99.99%) and cesium closo-dodecaborate ($Cs_2[closo\text{-}B_{12}H_{12}]$, 98%) were respectively purchased from Sinopharm Chemical Reagent Co., Ltd (Shanghai, China) and Strem Chemicals (Newburyport, USA). $MnCl_2 \cdot 4H_2O$, $FeCl_3 \cdot 4H_2O$, $Hg(NO_3)_2 \cdot 2H_2O$, $CoCl_2 \cdot 6H_2O$, $MgSO_4$, $CaCl_2 \cdot 2H_2O$, $AlCl_3$, $CrCl_3 \cdot 6H_2O$, $BaCl_2$ and $Pb(NO_3)_2$ were all of analytical grade and sourced from Aladdin Reagent (Shanghai, China). All metal ion reagents were prepared freshly before the experiment. To improve the sensitivity, 0.05 M of NaCl was added before the addition of metal ions. Reagent-grade NaOH (0.1 M) was used to adjust the pH value of solutions. Milli-Q ultra-pure water (18 MΩ cm^{-1}) was used to prepare all the solutions throughout the experiments.

Transmission electron microscopy (TEM) images were captured on a JEM-2100 microscope operated at 200 kV.

Scanning electron microscopy (SEM) images were taken on a field-emission microscope (Zeiss Sigma) operated at an accelerating voltage of 20 kV.

ESI-MS spectra were taken at room temperature on a mass spectrometer (Finnigan LCQ advantage; Thermo Fisher Scientific).

Ultraviolet-visible (UV-vis) extinction spectra were taken at room temperature on a spectrophotometer (TU-1901; Persee, Beijing, China) by use of quartz cuvettes with an optical path length of 1 cm.

X-ray powder diffraction (XRD) patterns were recorded on a Rigaku SmartLab diffractometer with a Cu-Kα radiation source (λ = 1.541 84 Å).

X-ray photoelectron spectra (XPS) were recorded using an electron spectroscope (Escalab 250Xi; Thermo Fisher Scientific) with an Al-Kα source (15 kV and 10 mA).

IR spectra were measured using a KBr plate in a Fourier transformation infrared (FTIR) spectrometer (Nexus 670; Thermo Nicolet Corporation, USA).

Zeta-potential was measured with a Zetasizer analyzer (Zen 3600; Malvern Instruments Ltd., Worcestershire, UK).

Microcalorimetric titration of lead ions with $[closo\text{-}B_{12}H_{12}]^{2-}$ (pH = 11) was measured with a VP-ITC Microcalorimeter (Microcal Inc., USA).

The Au ions were quantified using an inductively coupled plasma atomic emission spectrometer **(ICP-AES)** (IRIS Intrepid Ⅱ; Thermo Elemental, Franklin, USA).

2. General procedures for AuNPs formation

General procedure for the formation of [*closo*-$B_{12}H_{12}$]$^{2-}$-capped AuNPs with an average diameter of 15 nm: 1 mL of $HAuCl_4 \cdot 4H_2O$ (0.05 M) and 1 mL of Cs_2[*closo*-$B_{12}H_{12}$] (0.05 M) was added to H_2O at room temperature. The mixture turned faint red immediately and then stirred for 30 min continuously. The free Cs_2[*closo*-$B_{12}H_{12}$] in solution was removed by centrifugation at 12000 rpm for 15 min. The collected nanoparticle samples were washed and dispersed in H_2O.

3. Analytical data of [*closo*-$B_{12}H_{12}$]$^{2-}$-capped AuNPs

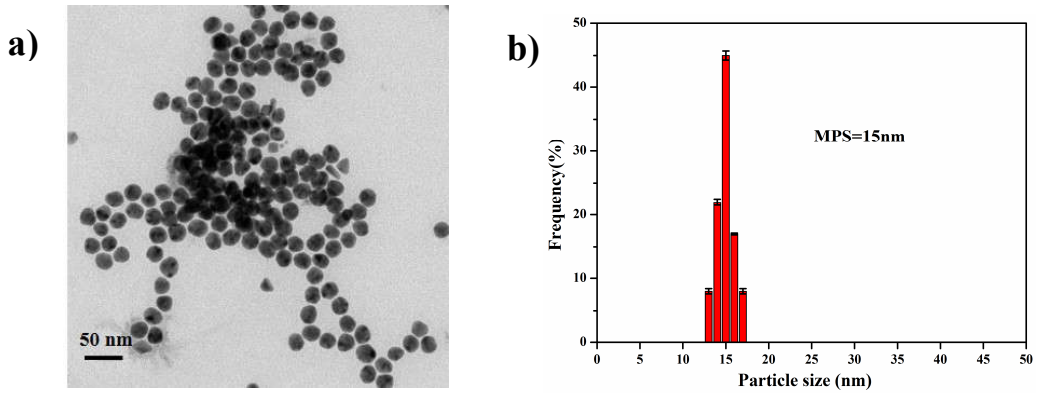

Figure S1. a) TEM micrograph of the AuNPs when the molar ratio of Cs_2[*closo*-$B_{12}H_{12}$] to $HAuCl_4$is 1; b) the corresponding particle size distribution. MPS is the mean particle size.

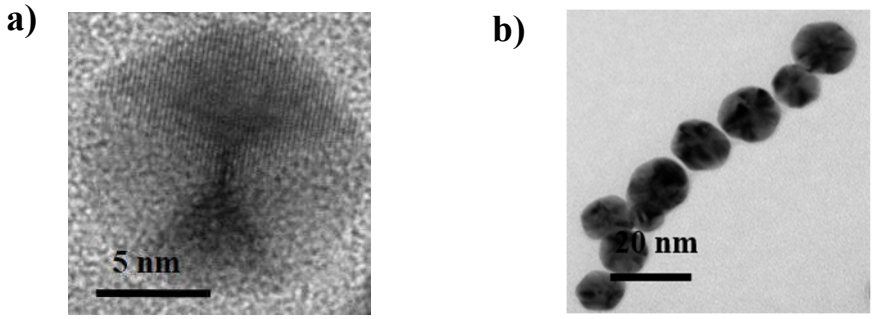

Figure S2. The HR-TEM (a) and TEM (B) images of AuNPs with defects–stacking faults and lattice distortions.

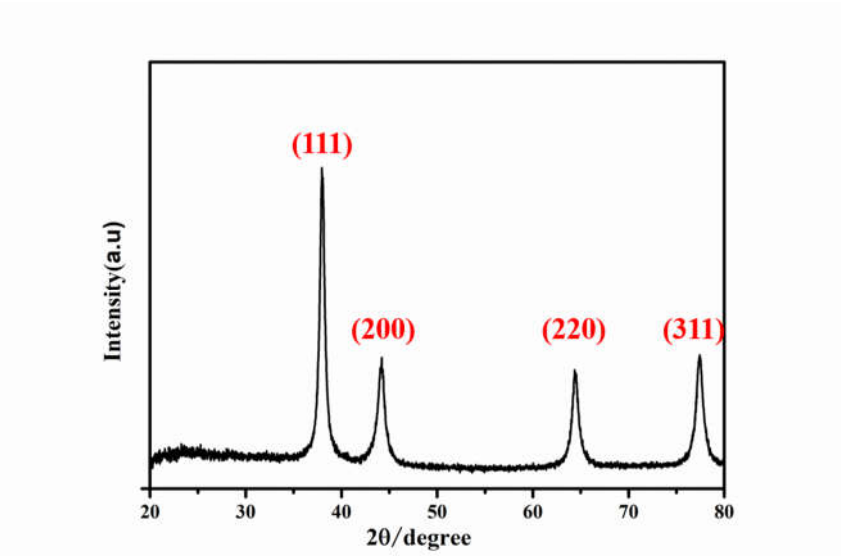

Figure S3. The X-ray diffraction (XRD) pattern spectrum of [*closo*-$B_{12}H_{12}$]$^{2-}$-capped AuNPs collected by centrifugation and vacuum drying.

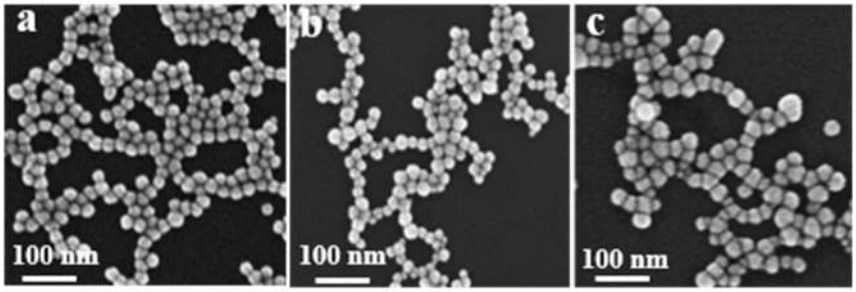

Figure S4. The SEM images of AuNPs at different concentration of $HAuCl_4$ with equal molar ratio of [*closo*-$B_{12}H_{12}$]$^{2-}$ to $HAuCl_4$ kept at 0.5: (a) 5×10^{-4} M, (b) 2×10^{-3} M, (c) 4×10^{-3} M.

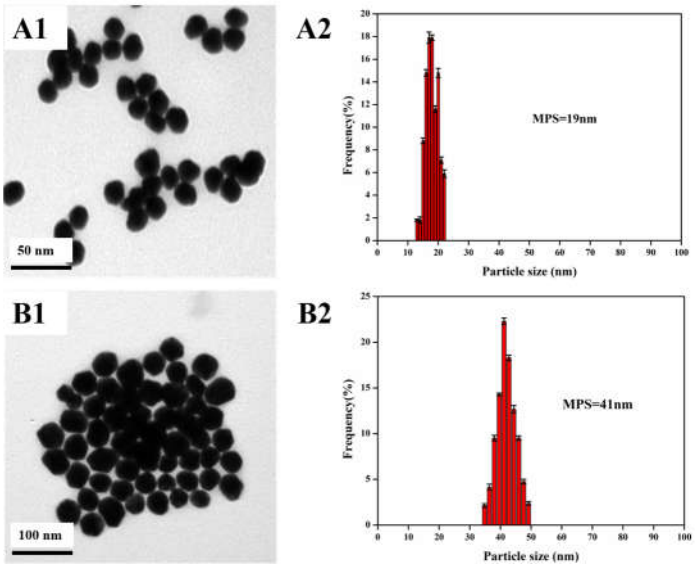

Figure S5. The TEM images of AuNPs at different molar ratio of [*closo*-$B_{12}H_{12}$]$^{2-}$ to $HAuCl_4$ with the same concentration of $HAuCl_4$ kept at 5×10^{-4} M: (A) 0.7; (B) 0.4.

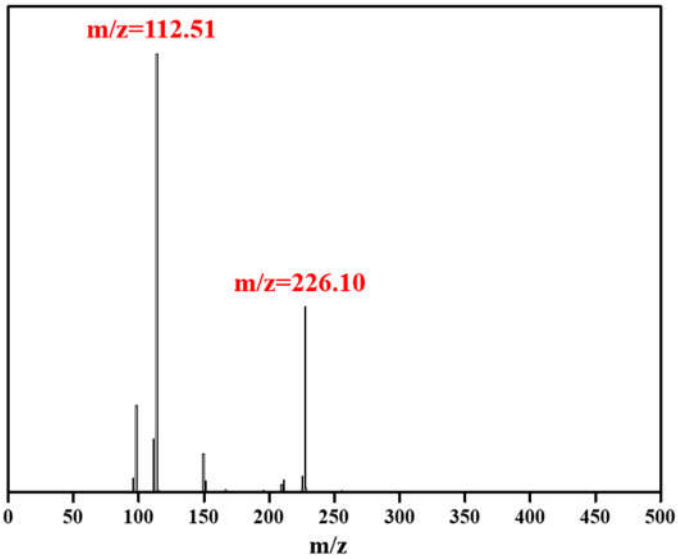

Figure S6. The ESI-MS spectrum of the oxidative products of [*closo*-$B_{12}H_{12}$]$^{2-}$.

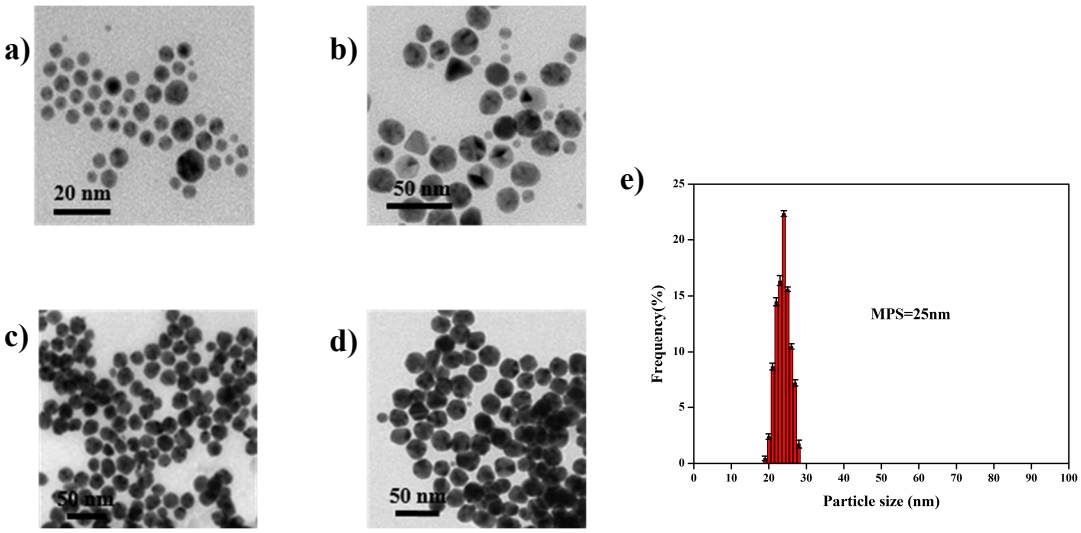

Figure S7. Time-dependent TEM micrographs over the course of reaction time when the molar ratio of Cs_2[*closo*-$B_{12}H_{12}$] to $HAuCl_4$ is 0.5: (a) 60s, (b) 5min, (c) 10min, (d) 30min; (e) the corresponding particle size distribution of (d).

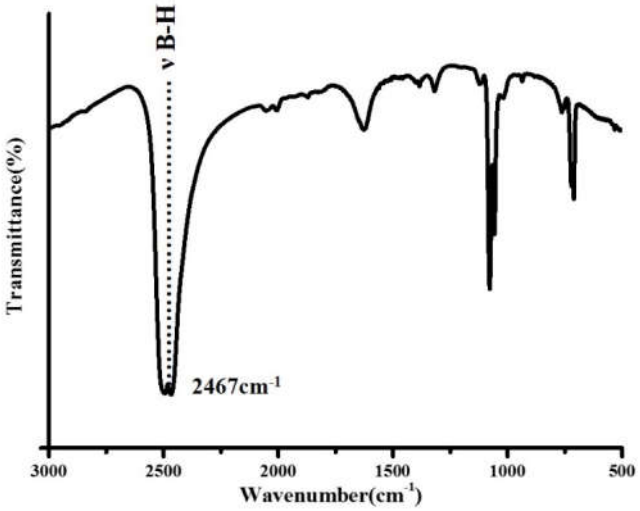

Figure S8. The FT-IR spectrum of [*closo*-$B_{12}H_{12}$]$^{2-}$-capped AuNPs collected by centrifugation and vacuum drying.

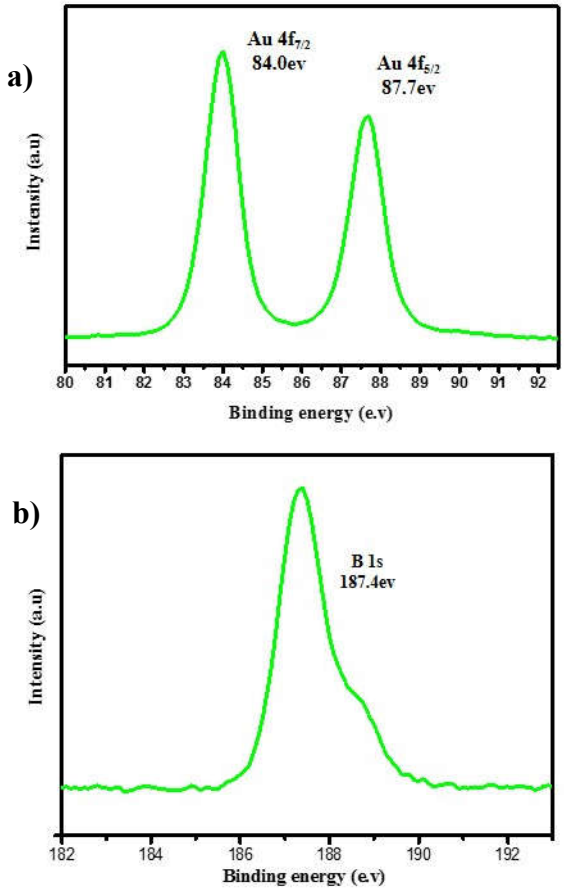

Figure S9. The XPS spectrums of Au 4f core-level for AuNPs (a) and boron 1s core-level for [*closo*-$B_{12}H_{12}$]$^{2-}$ (b).

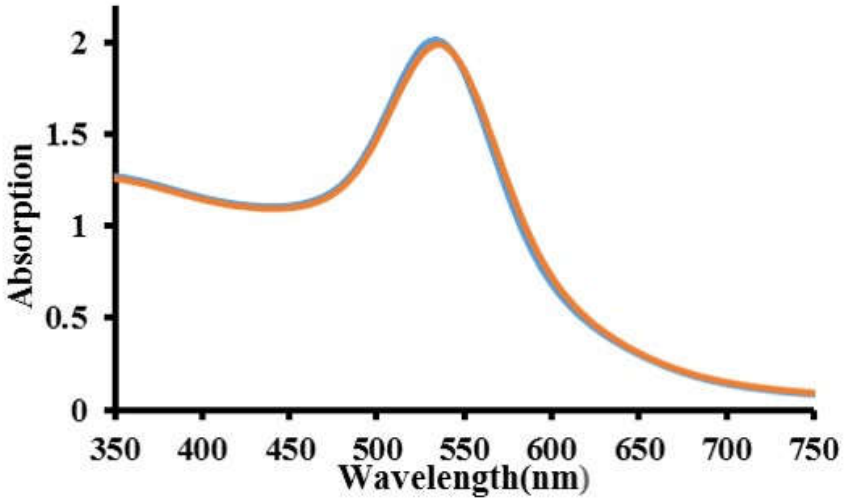

Figure S10. The UV-Vis spectra of gold nanoparticles: freshly prepared (red line) and kept for 3 months (blue line).

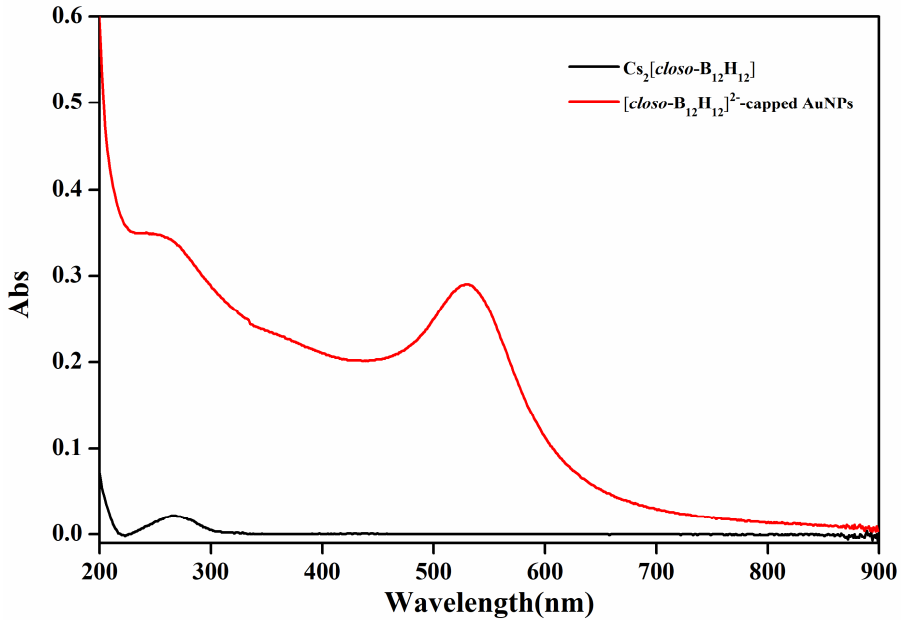

Figure S11. The UV-Vis spectra of Cs_2[*closo*-$B_{12}H_{12}$] and [*closo*-$B_{12}H_{12}$]$^{2-}$-capped AuNPs.

4. Phase transfer of [*closo*-$B_{12}H_{12}$]$^{2-}$-capped Au nanoparticles via exchanging cations of boron clusters

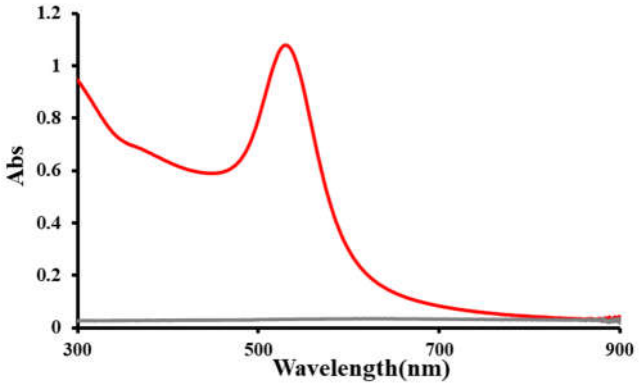

Figure S12. UV/Vis absorption spectra of [*closo*-$B_{12}H_{12}$]$^{2-}$-capped AuNPs colloid aqueous solution before (red) and after (grey) the addition of tetrabutylammonium bromide (TBAB).

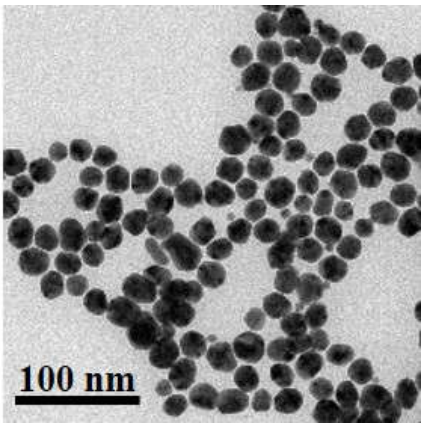

Figure S13. The TEM micrograph of the resulting organic solvent phase and the gold nanoparticles displayed no signs of degradation or aggregation.

5. General procedures for Cr (Ⅲ) and Pb (Ⅱ) detection

General procedures for metal ions detection: a series of metal ions (5 μM) were separately added to 6 μM of label-free [*closo*-$B_{12}H_{12}$]$^{2-}$-capped Au nanoparticles with an average of 15 nm in aqueous solution at pH 8.5 and 11. Before the addition of metal ions, 0.05 M NaCl was added to improve the sensitivity, which was expected to reduce the electrostatic repulsion among the negatively charged Au nanoparticles.[S1] The mixtures were then shaken by hand and determined by UV-vis spectrum after incubated at room temperature for 30 min. The pH of the solution was adjusted by addition of HCl (0.1 M) or NaOH (0.1 M) solution.

6. Analytical data of Cr (Ⅲ) and Pb (Ⅱ) detection based on [*closo*-$B_{12}H_{12}$]$^{2-}$-capped AuNPs

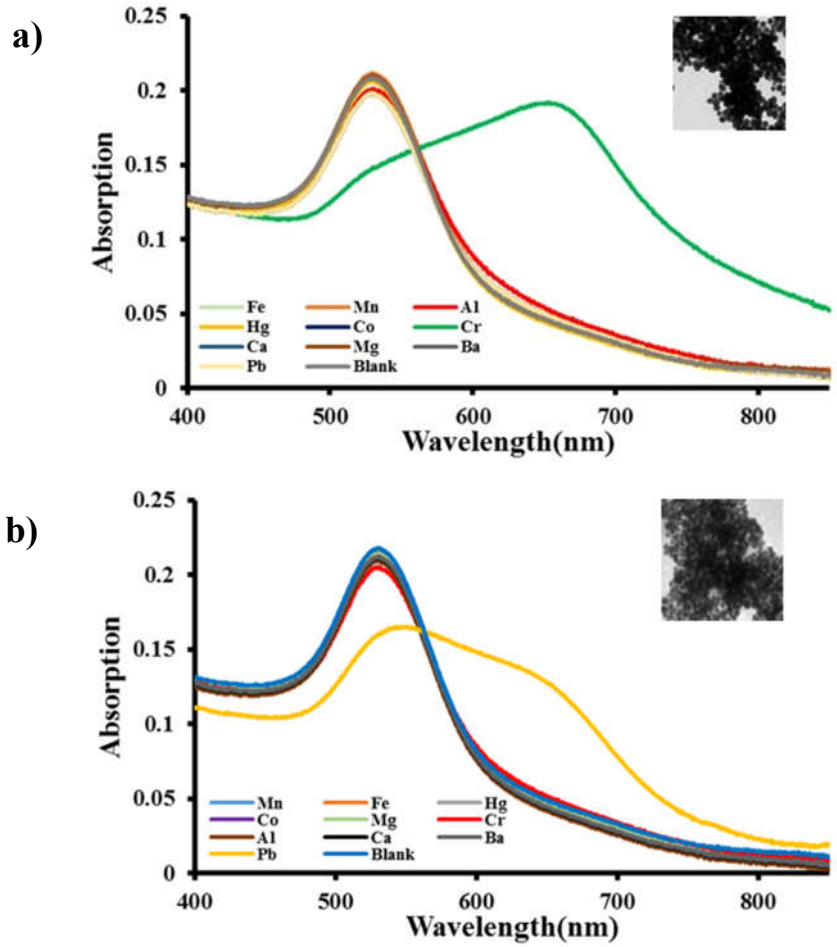

Figure S14. The UV-vis spectra of label-free Au decahedra after adding metal ions at different pH value of solution: (a) pH = 8.5 (inset: aggregated decahedral particles in the presence of Cr^{3+} ions); (b) pH = 11 (inset: aggregated decahedral particles in the presence of Pb^{2+} ions).

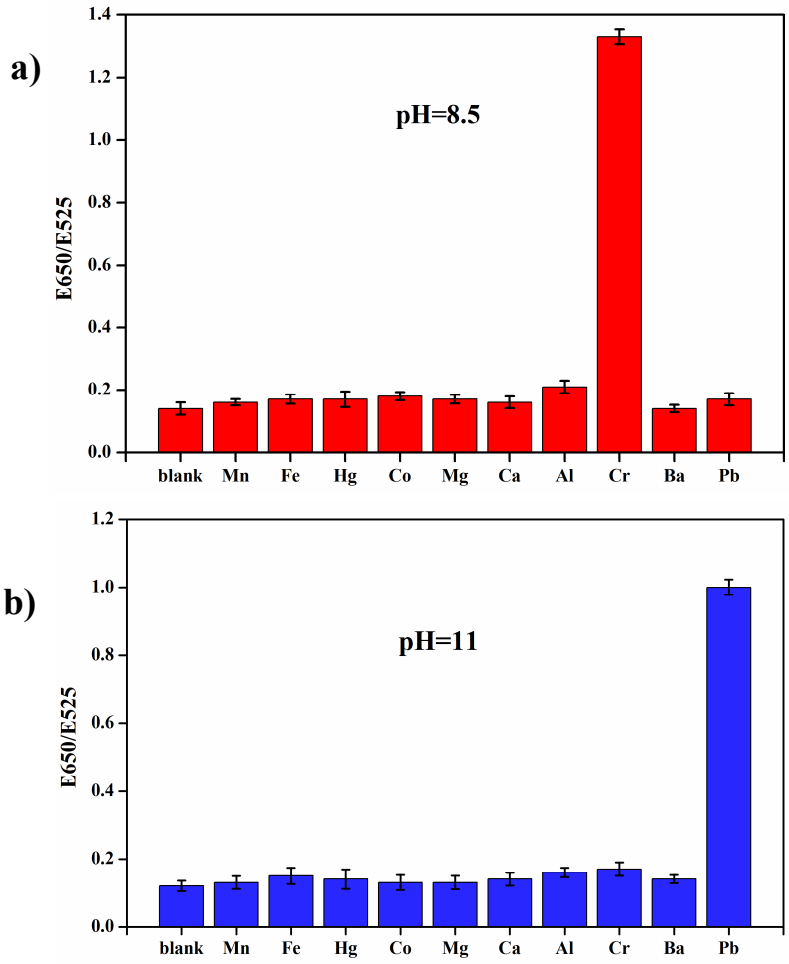

Figure S15. The extinctive ratios of intensity at 650 nm and 525 nm (E6500/E525) in the presence of 5 μM Mn^{2+}, Fe^{3+}, Hg^{2+}, Co^{2+}, Mg^{2+}, Ca^{2+}, Al^{3+}, Cr^{3+}, Ba^{2+} and Pb^{2+} ions at different pH value of solution with 0.05 M of NaCl: (a) pH=8.5; (b) pH=11.

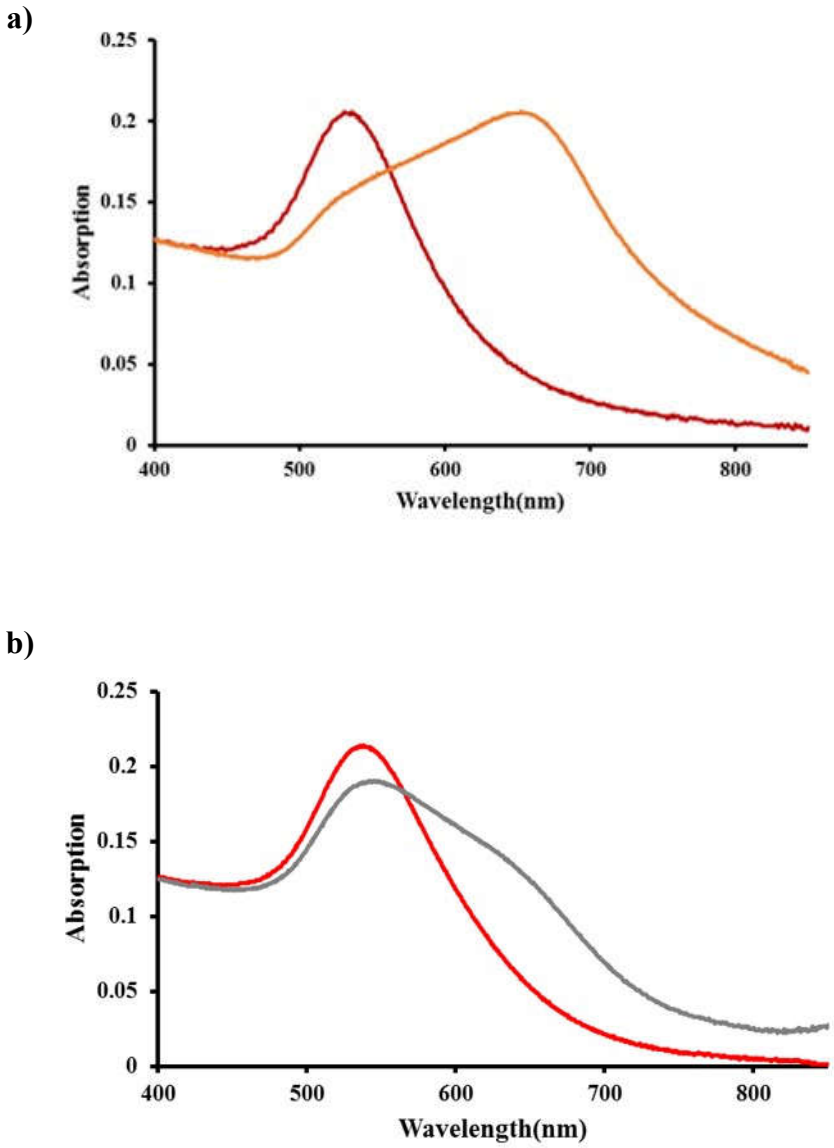

Figure S16. (a) The UV-Vis spectra of [*closo*-$B_{12}H_{12}$]$^{2-}$-capped AuNPs for colloidal solutions containing (Mn^{2+}, Fe^{3+}, Hg^{2+}, Co^{2+}, Mg^{2+}, Ca^{2+}, Al^{3+}, Ba^{2+} and Pb^{2+}) with (yellow line) and without (red line) Cr^{3+} at pH value of 8.5 with 0.05 M NaCl. (b) The UV-Vis spectra of [closo-$B_{12}H_{12}$]$^{2-}$-capped AuNPs for colloidal solutions containing (Mn^{2+}, Fe^{3+}, Hg^{2+}, Co^{2+}, Mg^{2+}, Ca^{2+}, Al^{3+}, Cr^{3+} and Ba^{2+}) with (gray line) and without (red line) Pb^{2+} at pH value of 11 with 0.05 M NaCl. The concentration of each metal ion was 1 μM.

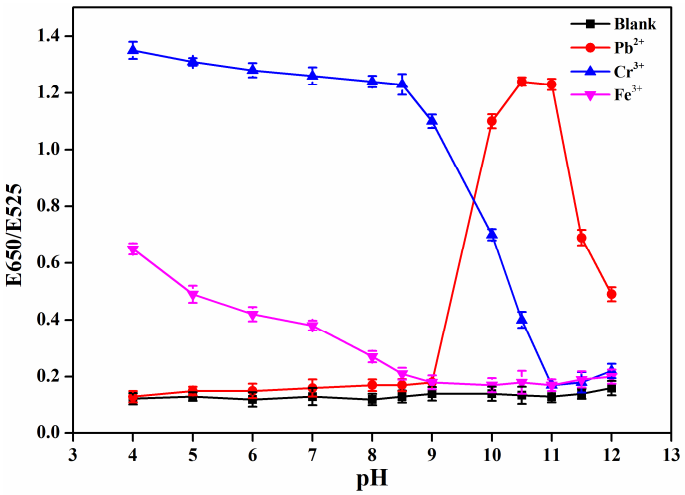

Figure S17. The extinctive ratios of intensity at 650 nm and 525 nm (E676/E520) in the presence of 50 μM Pb^{2+}, Cr^{3+} and Fe^{3+} ions versus pH value.

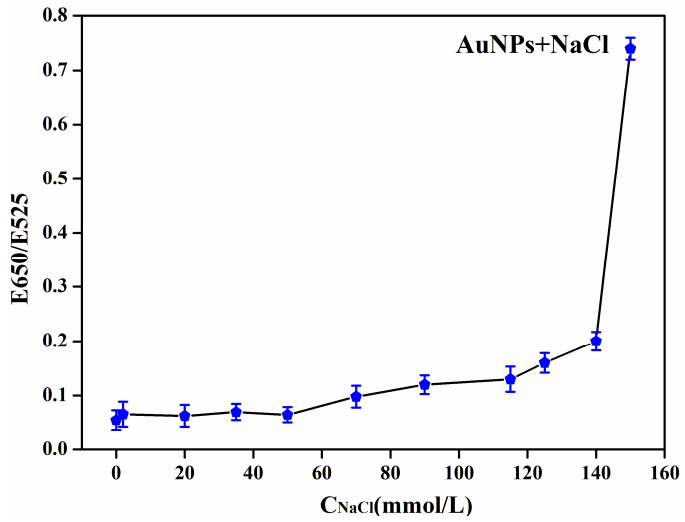

Figure S18. Plot of extinction ratio (E650/E525) versus the amount of NaCl.

7. [*closo*-$B_{12}H_{12}$]$^{2-}$-capped PtNPs and [*closo*-$B_{12}H_{12}$]$^{2-}$-capped AgNPs

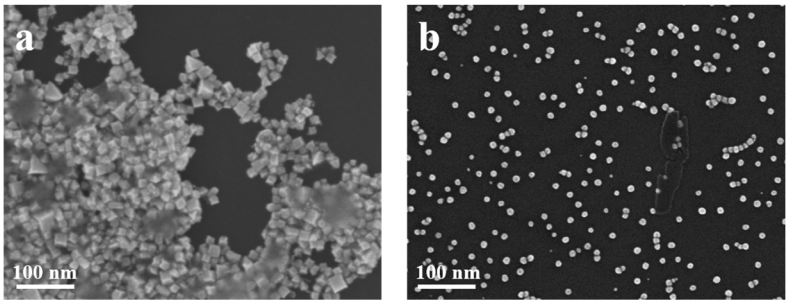

Figure S19. SEM images of (a) Pt nano-cubes and (b) sphere-like Ag nanoparticles prepared by means of the chemical reduction of metal salt precursor in an aqueous system, where Cs_2[closo-$B_{12}H_{12}$] was used both as an efficient reductant and stabilizer. These works are ongoing in our lab.

8. List of methods of colorimetric detection of Pb^{2+} and Cr^{3+}

Table S1. List of methods of colorimetric detection of Pb^{2+} and Cr^{3+}

Target	Probe	Readout	LOD/μM	Ref.
Pb^{2+}	DNA-AuNPs	Colorimetric/UV-vis	0.1	2
	DNAzyme-AuNPs	Colorimetric	0.5	3
	GA-AuNPs	Colorimetric/UV-vis	5	4
	MUA-AuNPs	Colorimetric/UV-vis	10	5
	this work	Colorimetric/UV-vis	**0.02**	/
Cr^{3+}	DTNBA-AuNPs	Colorimetric/UV-vis	1.8	6
	NTP-AuNPs	Colorimetric/UV-vis	1.4	7
	DMSA-AuNPs	Colorimetric/UV-vis	0.01	8
	this work	Colorimetric/UV-vis	**0.005**	/

9. References

[1] J. Guan, W. S. Yang, *Colloids and Surfaces A: Physicochem. Eng. Aspects.* **2008**, *325*, 194–197.

[2] J. W. Liu, Y. Lu, *J. Am. Chem. Soc.,* 2004, **126**, 12298–12305.

[3] D, Mazumdar, J. W. Liu, G. Lu, J. Z Zhou, Y. Lu, *Chem. Commun.,* 2010, **46**, 1416–1418.

[4] K. Yoosaf, B. I. Ipe, C. H. Suresh, K. G. Thomas, *J. Phys. Chem. C,* 2007, **111**, 12839–12847.

[5] C. H. Fan, S. J. He, G. Liu, L. H. Wang, S. P. Song, *Sensors*, 2012, **1**2, 9467-9475.

[6] Y. Q. Dang, H. W. Li, B. Wang, L. Li, Y. Q. Wu, *ACS Appl. Mater. Interfaces,* 2009, **1**, 1533–1538.

[7] Y. C. Chen, I. L. Lee, Y. M. Sung, S. P. Wu, *Sens. Actuators, B,* 2013, **188**, 354-359.

[8] W. W. Chen, Z. Wang, K. Deng, X. Y. Jiang, *Nanoscale*, 2015, **7**, 2042–2049.